View metadata, citation and similar papers at core.ac.uk
brought to you by CORE
provided by University of Hertfordshire Research Archive

Mon. Not. R. Astron. Soc. **000**, 1–?? (2002) Printed 29 March 2007 (MN LaTeX style file v2.2)

Probing the Sagittarius stream with blue horizontal branch stars

L. Clewley⋆ & Matt J. Jarvis†
Astrophysics, Department of Physics, Keble Road, Oxford, OX1 3RH, UK

arXiv:astro-ph/0601674v1 30 Jan 2006

Released 2002 Xxxxx XX

ABSTRACT

We present 2-degree field spectroscopic observations of a sample of 96 A–type stars selected from the Sloan Digital Sky Survey Data Release 3 (SDSS DR3). Our aim is to identify blue horizontal branch (BHB) stars in order to measure the kinematic properties of the tidal tails of the Sagittarius dwarf spheroidal galaxy. We confine our attention to the 44 classifiable stars with spectra of signal-to-noise ratio $> 15\text{Å}^{-1}$. Classification produces a sample of 29 BHB stars at distances $5 - 47$ kpc from the Sun. We split our sample into three bins based on their distance. We find 10 of the 12 stars at $14 - 25$ kpc appear to have coherent, smoothly varying radial velocities which are plausibly associated with old debris in the Sagittarius tidal stream. Further observations along the orbit and at greater distances are required to trace the full extent of this structure on the sky. Three of our BHB stars in the direction of the globular cluster Palomar (Pal) 5 appear to be in an overdensity but are in the foreground of Pal 5. More observations are required around this overdensity to establish any relation to Pal 5 and/or the Sgr stream. We emphasize observations of BHB stars have unlimited potential for providing accurate velocity and distance information in old distant halo streams and globular clusters alike. The next generation multi-object spectrographs provide an excellent opportunity to accurately trace the full extent of such structures.

Key words: galaxies: individual (Sagittarius) – Galaxy: halo – stars: horizontal branch – Galaxy: structure – Galaxy: stream

1 INTRODUCTION

There have been numerous searches for streams of material responsible for the build-up of stellar halos in galaxies. In the Milky Way the best studied is the Sagittarius (Sgr) dwarf spheroidal galaxy (Ibata, Gilmore & Irwin 1994) and its stellar stream (e.g. Majewski et al. 2003). An extended stream of stars has also been uncovered in the halo of the Andromeda galaxy (M31), revealing that it too is cannibalizing a small companion (e.g. Lewis et al. 2004). Such streams yield crucial information on the merging and accretion history of galaxy halos and have been used to constrain the mass of the Milky Way halo (e.g. Johnston et al. 1999) and the mass of the halo in M31 (Ibata et al. 2004).

There are numerous studies reporting stellar streams associated with the tidal debris of the Sgr system either trailing or leading it along its orbit. The stars involved in the tidal disruptions can be used as test particles which can lead to an understanding of the shape (Helmi 2004) and strength of the Milky Way potential. A number of studies have sought to trace Sgr and its stream with a variety of stellar populations. For example, Totten & Irwin (1998) found evidence for such streams using intrinsically rare, but very luminous, carbon stars. The calibration of the carbon star distance scale remains controversial and is further complicated by variability, dust and metallicity effects. Numerous RR Lyrae stars have also been found to be associated with the Sgr stream (Ivezić et al. 2000; Vivas et al. 2001; Vivas et al. 2005). The Quasar Equatorial Survey Team (QUEST) survey (Vivas at al. 2004) found 85 RR Lyrae variables covering about 36° in right ascension, of which 16 were identified spectroscopically (Vivas et al. 2005). An all-sky view of the Sgr stream has been investigated using M giants selected from the Two Micron All-Sky Survey (2MASS) database (Majewski et al. 2003, 2004).

There is strength in diversity. Heterogeneous stellar populations not only provide an important check on the distance and velocity measurements of any putative stream but also probe different formation epochs. Blue Horizontal Branch (BHB) stars provide yet another stellar population ideal for exploring Halo structure (Sirko et al. 2004; Brown et al., 2004; Clewley et al., 2005). Newberg at al. (2002) find a distant sample of BHB stars that, they suggest, reside in

⋆ clewley@astro.ox.ac.uk
† mjj@astro.ox.ac.uk

the trailing arm of the Sgr stream. Further, Monaco et al. (2003) suggest that a sample of BHB stars discovered in the core of the Sgr dwarf spheroidal galaxy are the counterpart of the stars observed by Newberg et al. (2002).

Both BHB stars and RR Lyraes are excellent standard candles, enabling us to determine their distances to 5-10%; by contrast the distances to K and M giants are accurate to 20% - 25% (e.g. Dohm-Palmer et al. 2001; Majewski et al. 2003). BHB and RR Lyrae stars are also old and metal poor, so they are ideal for tracing old parts (> 5 Gyr) of tidal streams. The age of the Sgr M giants is controversial. Majewski et al. 2003 considered these stars to be younger than 5 Gyr with a significant fraction of them only $2-3$ Gyrs old (Majewski et al. 2003). This poses two problems for their use as tracers. First, they may not be useful halo test particles as such dynamically young tracers do not place very stringent constraints on the halo (Helmi 2004). Second, comparisons between the evolution timescales of the M giants and the dynamical timescale required for the stars to populate the stream suggest that the stars exist in a stream that took more than their age to form. This inconsistency has been addressed by Bellazzini et al. (2005) who finds the M giants were considerably older (> 5 Gyr) than was originally thought and may even probe similar epochs as RR Lyraes or BHB stars.

This paper is the first in a series that discusses the use of BHB stars to directly trace the Sgr stream. BHB stars are A–type giants that are easily identified in the Galactic halo as they lie blueward of the main–sequence turnoff (e.g. Yanny et al. 2000). Assembling clean samples of remote BHB stars has been stymied by the existence of a contaminating population of high–surface–gravity A–type stars, the blue stragglers, that are around two magnitudes fainter. Previous analyses required high signal-to-noise ratio (S/N) spectroscopy to reliably separate these populations (e.g. Kinman, Suntzeff & Kraft 1994), making identification of BHB stars in the distant halo unfeasible. However, recently Clewley et al. (2002, 2004) developed two classification methods that now enable us to overcome the difficulties of cleanly separating BHB stars from blue stragglers.

In this paper we use these classification techniques, and the Sloan Digital Sky Survey Data Release 3 (SDSS DR3) photometry, to isolate a sample of BHB stars along the Sgr stream. In this new survey we target stars along the equatorial strip in the region $180^\circ <$RA$< 249^\circ$, which are sensitive to the different models that distinguish between halo flatness using the Sgr stream (e.g. Martínez-Delgado et al. 2004).

In Section 2 of this paper we describe the selection of the BHB candidates from the SDSS data set, and outline the prescription for transforming the SDSS g, r magnitudes of A–type stars to B, V magnitudes detailed in Clewley et al. (2005). Section 3 provides a summary of the 2dF spectroscopic observations and data reduction procedures. In Section 4 we classify these stars into categories BHB and blue straggler. Section 5 presents the results of the classification procedure and provides a summary table of distances and radial velocities of the stars classified as BHB. Three BHB stars in the direction of the globular cluster Pal 5 appear to be in an overdensity but in the foreground of Pal 5; we compare our measurements with those in the literature. In Section 6 we investigate the evidence that the stars reside in a stream and are associated with the Sgr tidal debris.

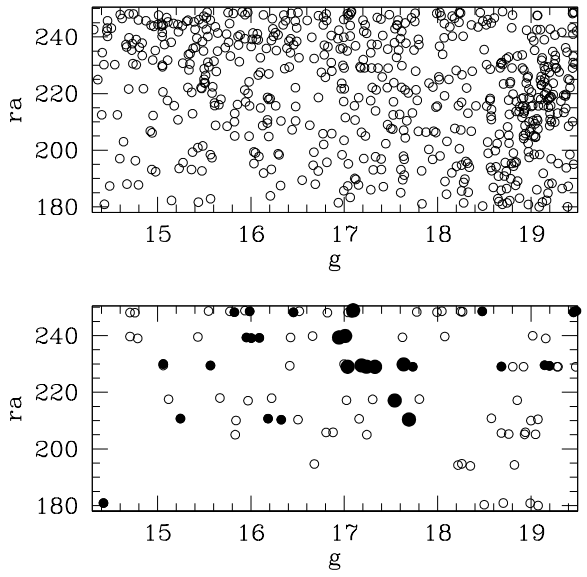

Figure 1. *Upper:* A plot of RA against g for all the BHB star candidates in the SDSS satisfying our selection criteria (detailed in the text). Selection was confined to the equatorial strip and the range $180^\circ <$RA$< 250^\circ$. There are 610 stars satisfying the selection criteria. *Lower:* A plot of RA against g for the 96 stars observed. The coordinates of the eight pointings are provided in Table 1. Filled circles are stars that are classified BHB. The large filled circles are candidate stream members.

Finally, in Section 7 we provide a summary of the main conclusions of the paper. In this paper we use the coordinate R_{gal} to denote Galactocentric distances and the coordinate $R_\odot$ to denote heliocentric distances.

2 SELECTING THE BHB CANDIDATES

2.1 Colour selection

Our aim was to use the SDSS photometric data to select a sample of candidate faint BHB stars, with minimal contamination by quasi-stellar objects (QSOs) and F–type stars. We selected the candidate BHB stars using the SDSS point spread function (PSF) *ugr* magnitudes of stellar objects. The SDSS is 95% complete for point sources to (u, g, r, i, z) = (22.0, 22.2, 22.2, 21.3, 20.5) and is saturated at about 14 magnitudes in g, r and i and about 12 mag. in u. Consequently, we select stars with $14.3 < g < 19.5$. The fainter limit was added in retrospect and is a consequence of the 2dF instrument capability and the observing conditions coupled with our strict signal-to-noise (S/N) requirements for classification, which we outline below. All the SDSS magnitudes discussed in this paper have been corrected for Galactic extinction, using the map of Schlegel, Finkbeiner & Davis (1998). We limited ourselves to the equatorial stripe in the SDSS data set which is observable from the southern hemisphere, with $180^\circ <$ RA $< 249^\circ$ (J2000).

In selecting candidate distant BHB stars from the SDSS, we used the results of Yanny et al. (2000), who studied the spatial distribution of a sample of A–type stars selected from the SDSS using the (reddening–corrected) colour

No.	l	b	RA J 2000
01	277.27	60.38	12 02
02	329.12	60.28	13 42
03	345.38	55.23	14 22
04	355.34	49.97	14 54
05	1.42	45.57	15 18
06	6.59	40.90	15 42
07	9.64	37.66	15 58
08	15.00	31.00	16 30

Table 1. Galactic and equatorial coordinates of the centres of the eight fields observed in the survey, ordered by Right Ascension. The declination of all eight fields are centered along the equator.

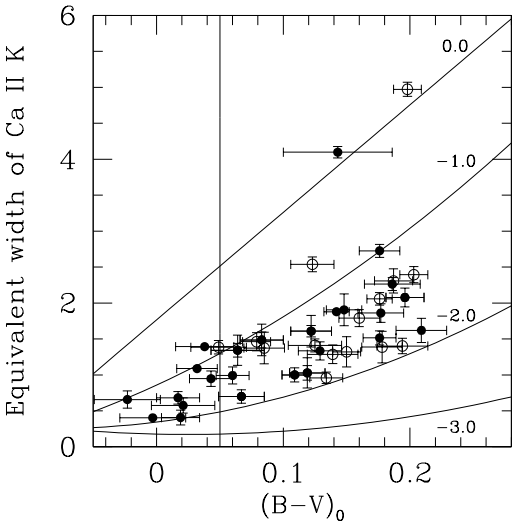

Figure 2. CaII K line (3933 Å) EW(Å) for the sample plotted against $(B-V)_0$. The curves represent lines of constant metallicity for [Fe/H] = -1.0, -2.0 and -3.0 taken from Wilhelm et al. (1999). The straight line represents a best fit to stars in the Pleiades and Coma clusters assumed to be of solar metallicity. The vertical line at $(B-V)_0 = 0.05$ is the limit for which metallicities can be determined. The 29 stars classified as BHB stars are marked by filled circles, the 15 stars classified blue straggler are marked by open circles.

selection box $-0.3 < g-r < 0.0$, $0.8 < u-g < 1.4$. On this basis, we adopted the colour cuts defined by Yanny et al. (2000), and limited candidate selection to objects with colour error $\sigma(g-r) < 0.07$. There are 610 objects in this sample. While these colour cuts should be nearly optimal in terms of the fraction of candidates that are A–type stars, we still expect substantial contamination by blue stragglers.

We use two methods to classify stars into categories BHB and blue straggler. As one method makes use of $(B-V)_0$ colours we need to convert the extinction corrected $g-r$ colours to $B-V$. In Clewley et al. (2005) we described a reinvestigation of this conversion and compared it to Fukugita et al. (1996) and Smith (2002). We derived a cubic relation that provides an improved fit. The transformation is given by

$$B-V = 0.764(g-r) - 0.170(g-r)^2 + 0.715(g-r)^3 + 0.218. \quad (1)$$

We stress that this relation is specifically for A–type stars, and is not expected to be reliable for other types of star.

We chose 8 pointings roughly equidistant in RA along the stream. The coordinates of the centres of the pointings are provided in Table 1. The final selection includes 96 A–type stars which are listed in Table 2. In this table Column 1 is our running number, and column 2 lists the coordinates. Successive columns provide the dereddened SDSS g magnitude, and the dereddened $u-g$ and $g-r$ colours. The last column provides the dereddened $B-V$ colour, calculated using the transformation shown in Equation 1.

Looking ahead, our classification methods were developed specifically for objects with strong Balmer lines, defined by EW H$\gamma > 13$Å, and with a signal-to-noise (S/N) in the continuum > 15Å^{-1}. Of the 96 selected candidates we are able to adequately classify 44 stars, of these 29 were classified BHB. For the 52 stars that we are unable to classify the majority (37 stars) were because the S/N was insufficient. In addition, there were 4 QSOs and 11 stars with EW H$\gamma < 13$Å.

Figure 1 shows the distribution in RA and g magnitude of the selections. In Figure 1(lower) the 96 colour selected stars are shown as open circles with solid circles representing the 29 stars that are classified BHB. The horizontal stripes represent the pointings.

3 SPECTROSCOPIC OBSERVATIONS

Medium resolution spectra were obtained for the 96 candidates in eight pointings spread over four nights from 11-14 May 2005 using the two-degree field (2dF; Lewis et al. 2002) multi-object spectrograph on the 3.9-m Anglo-Australian Telescope (AAT). The instrument was equipped with a 2048^2 Tek CCD, with a projected scale of $0.2''$pixel^{-1}. We used the R1200B grating, giving a dispersion of 1.1 Å pixel^{-1} and a spectral coverage of 3800–4900 Å, which includes the relevant lines Hδ, Hγ, and Ca II K λ3933Å. With the $1''$fibres the FWHM resolution, measured by fitting Gaussian profiles to strong unblended arc lines, was 2.6 Å which is sufficient for the line–fitting procedure. Four BHB radial velocity standard stars in the globular cluster M5 were also observed nightly. Table 3 summarizes relevant information for the standards. This table provides a list of the identification, RA and Dec., V magnitude, $(B-V)_0$ colour, and the heliocentric radial velocity, $V_\odot$. Successive columns (6) to (11) in Table 3 contain averages of $H\delta$ and $H\gamma$ lines measured from a Sérsic function discussed in more detail in §4.

Total integration times between 7200 and 12000 seconds were chosen (split into 2400 second exposures) using the 2dF exposure-time calculator, based on the seeing, transparency, and lunar phase. This was done in order to achieve a minimum continuum S/N ratio of 15 Å^{-1}, which was required to classify the stars (Clewley et al. 2002). In the event, observations of 37 of the 96 targets failed to achieve the required S/N, and therefore these targets cannot be reliably classified. The failures were primarily in the cases where the seeing was poor and the targets were faint. All targets were observed near culmination, with a mean airmass of 1.2 ± 0.1.

No. (1)	Identification (J2000) (2)	g (3)	$(u-g)_0$ (4)	$(g-r)_0$ (5)	$(B-V)_0$ (6)
01	J120341.440+001400.96	18.703 ± 0.020	1.092 ± 0.037	-0.024 ± 0.026	0.200 ± 0.0200
02	J155953.064+002931.70	19.018 ± 0.015	1.078 ± 0.054	-0.094 ± 0.021	0.144 ± 0.0169
03	J163544.242+001048.25	17.095 ± 0.010	1.132 ± 0.023	-0.192 ± 0.014	0.060 ± 0.0126
04	J143156.510+001251.44	15.668 ± 0.022	1.105 ± 0.030	-0.117 ± 0.026	0.125 ± 0.0214
05	J151955.913+001617.05	15.061 ± 0.015	1.204 ± 0.017	-0.054 ± 0.020	0.176 ± 0.0157
06	J120339.027+000522.44	14.421 ± 0.046	1.338 ± 0.060	-0.096 ± 0.054	0.143 ± 0.0431
07	J163518.461-001113.78	15.936 ± 0.008	1.051 ± 0.020	-0.224 ± 0.012	0.031 ± 0.0113
08	J125902.040+001331.21	18.259 ± 0.022	1.236 ± 0.039	-0.212 ± 0.033	0.042 ± 0.0301
09	J134332.838+001243.41	18.940 ± 0.018	1.184 ± 0.048	-0.093 ± 0.025	0.145 ± 0.0201

Table 2. Photometric data for the 96 target BHB candidates taken from the SDSS. Column (1) is our running number, column (2) lists the coordinates. Columns (3) to (5) list the dereddened g magnitude, $u-g$, $g-r$ colours. The last column provides the $(B-V)_0$ colour. The table is presented in its entirety in the electronic edition of Monthly Notices.

The image frames were reduced with the 2dF pipeline (2dfDR v3.31, Bailey et al. 2003). This package carries out bias subtraction, flat-fielding, tram-line mapping to the fibre locations on the CCD, fibre extraction, arc identification and wavelength calibration. For the tram-line mapping and wavelength calibration, fibre flat-field frames and CuAr arc observations were made before and after each 45 min exposure. The arcs were used to derive accurate positions of the spectra on the CCD and to calculate the time-varying dispersion solution due to flexure of the instrument. This approach was very successful. We found, from the scatter of the radial velocity standard stars (table 3), a *rms* drift in the zero point of $9\,\mathrm{kms}^{-1}$ over the entire data set.

4 SPECTROSCOPIC ANALYSIS AND CLASSIFICATION

4.1 Analysis

The spectra were used, in combination with the photometry, to classify the stars, measure the metallicity and calculate the radial velocities. For these measurements we followed the procedures set out in Clewley et al. (2002, 2004) exactly, and we refer the reader to those papers for full details. Below we briefly summarize the procedures we undertake to measure the Balmer lines, metallicities and distances.

For the Balmer lines we normalized each spectrum to the continuum, and fitted a Sérsic function, convolved with a Gaussian that has the FWHM of the instrumental resolution. We have two classification procedures. First, the *Scale width–Shape* method, plots the scale width b, and the shape index c. Second, the $D_{0.15}$*–Colour* method plots $D_{0.15}$, which is the line width at a depth 15% below the continuum against $(B-V)_0$.

With some exceptions (including the A metallic (Am) and peculiar (Ap) stars) the strength of the Ca II K line at constant temperature can be used as an indicator of the metallicity of A-type stars (e.g. Pier 1983, Beers et al. 1992, Kinman et al. 1994). The metallicities were determined from the Ca II K 3933Å , line by minimum$-\chi^2$ fitting a Gaussian to the continuum divided spectrum over the wavelength range 3919–3949 Å. The metallicities were derived by plotting Ca II K line EW against $(B-V)_0$ and interpolating between lines of constant metallicity (see Figure 2). The uncertainty is established from the uncertainties of the two quantities plotted, and an additional uncertainty of 0.3dex is added in quadrature. This systematic error was established by using our methods on high S/N stars with known metallicities. As the lines in Figure 2 converge towards the bluer colours we consider this plot only reliable for colours redder than $(B-V)_0 > 0.05$. No attempt has been made to remove the possible contribution of interstellar Ca II K absorption from the stellar K measurements.

The absolute magnitudes of BHB stars, $M_V(BHB)$, depend on both metallicity and colour (i.e. temperature). Preston, Shectman & Beers (1991) provided an empirical Luminosity-Colour relation for BHB stars derived from a fit to globular cluster BHB stars. Recently, this empirical relation was re-investigated by Brown et al. (2005), who provided a physical basis for this relationship based on theoretical modelling. In Clewley et al. (2004) we derived a relation for the absolute magnitude of BHBs in two steps. First, we used the results from the Clementini et al. (2003) to determine the slope of the relation, $M_V(RR) = \alpha + \beta[\mathrm{Fe/H}]$. We fixed the zero point of the relation using the measurement by Gould & Popowski (1998) of the absolute magnitude of RR Lyrae stars, $M_V(RR) = 0.77 \pm 0.13$ mag at [Fe/H] = -1.60, derived from statistical parallaxes of *Hipparcos* observations. Combining these two measurements resulted in $M_V(RR) = 1.112 + 0.214[\mathrm{Fe/H}]$. Second we adopted the cubic expression determined by Preston et al. (1991) for the $(B-V)_0$ colour dependence of the difference in absolute magnitudes between BHB and RR Lyrae stars. This produced the final expression for the absolute magnitude of BHB stars:

$$\begin{aligned} M_V(BHB) &= 1.552 + 0.214[\mathrm{Fe/H}] - 4.423(B-V)_0 \\ &\quad +17.74(B-V)_0^2 - 35.73(B-V)_0^3. \end{aligned} \qquad (2)$$

Distances and associated errors are then determined using the apparent magnitudes V_0, and the corresponding photometric and metallicity errors. To compute V, we used the relation $V = g' - 0.53(g'-r')$ (Fukugita et al. 1996), here disregarding the subtle differences between the different SDSS magnitudes (g, g', g^*, etc.). The result produces distance errors of $6-10\%$ for our confirmed BHB stars. We caution that the M_V–metallicity relation is still controversial and so distance measurements may be systematically in error. We

ID	RA (J2000) Dec.	V_0	$(B-V)_0$	$V_\odot$ [km s^{-1}]	$D_{0.15}(\gamma\delta)$ [Å]	$b(\gamma\delta)$ [Å]	$c(\gamma\delta)$	A	B	θ
(1)	(2)	(3)	(4)	(5)	(6)	(7)	(8)	(9)	(10)	(11)
M5-II-78	J151826.93 + 020717.78	14.95	0.12	42.2 ± 1.1	30.322 ± 0.501	7.778	0.799	0.196	0.021	1.5139
					30.276 ± 0.459	7.966	0.829	0.184	0.021	1.5131
M5-IV-05	J151835.34 + 020227.94	15.15	0.15	56.9 ± 1.2	31.675 ± 0.482	8.365	0.836	0.192	0.020	1.5164
					31.510 ± 0.500	8.421	0.851	0.197	0.022	1.5171
M5-III-69	J151830.43 + 020224.57	15.06	0.18	56.2 ± 1.5	28.654 ± 0.489	7.196	0.775	0.189	0.020	1.5113
					29.282 ± 0.465	7.248	0.754	0.179	0.018	1.5131
M5-I-53	J151836.35 + 020744.60	15.06	0.06	52.2 ± 1.4	31.966 ± 0.454	8.372	0.827	0.182	0.019	1.5173

Table 3. Spectroscopic measurements of four M5 globular cluster BHB stars. The names are from Arp (1955) and Arp (1962), the photometry is from Cudworth (1979), and the radial velocities are from Peterson (1983). Columns (1) and (2) are the number and coordinates. Columns (3) and (4) list the dereddened V magnitude and $B-V$ colours. The radial velocity, corrected to the heliocentric frame, is provided in column (5). Successive columns (6) to (11) contain averages of $H\delta$ and $H\gamma$ line measurements measured from a Sérsic function. Column (6) is the line width at a depth 15% below the continuum and the parameters in (7) and (8) are the scale width (b), and the shape index (c). The errors in these latter two quantities are shown in (9) to (11), these are A and B, the semi-major and semi-minor axes of the error ellipse in the $b-c$ plane, and θ the orientation of the semi-major axis, measured anti-clockwise from the b-axis. Here the error corresponds to the 68% confidence interval for each axis in isolation [see Clewley et al. (2002) for further details].

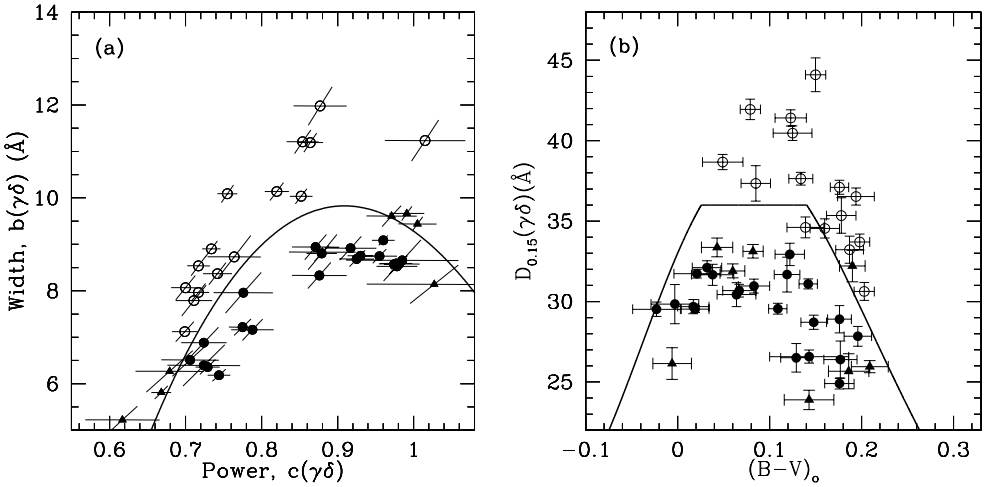

Figure 3. Classification of all 44 stars with unambiguous classifications shown in Table 4, using the (a) the *Scale width–Shape* and (b) $D_{0.15}$*–Colour* classification methods. The solid curves are the classification boundaries explained in the text. Filled circles are stars classified BHB in both plots, i.e. the stars below the classification boundary in each plot. Open circles are stars classified A/BS. Filled triangles are stars below the classification boundary in only one plot but are nonetheless classified BHB. In plot (a) there are 23 stars below the boundary and 21 above it. In plot (b) there are 29 stars below the boundary and 15 above it. A total of 29 stars are classified BHB.

refer the interested reader to a recent review of this subject by Cacciari & Clementini (2003) and Alves (2004).

The absolute magnitudes of blue stragglers have been less well studied. As we do not analyse them here we simply adopt the relation, $M_V(BS) = 1.32 + 4.05(B-V)_0 - 0.45$[Fe/H], derived by Kinman et al. (1994).

4.2 Classification

In Figure 3 we plot the two diagnostic diagrams for the 44 classifiable stars in the survey. Figure 3(a) shows the *Scale width–Shape* method. The line–profile quantities b and c, averaged for Hγ and Hδ are plotted. Figure 3(b) shows the $D_{0.15}-$*colour* method. Plotted are values of $D_{0.15}$ for Hγ and Hδ against $(B-V)_0$ for all the stars. The solid lines show the classification boundaries, taken from Clewley et al. (2002, 2004), with high–surface gravity stars (i.e. main–sequence A stars or blue stragglers, hereafter A/BS) above the line, and low–surface gravity stars (i.e. BHB stars) below the line. In both plots stars classified BHB are plotted as solid symbols and stars classified A/BS are plotted open. As we discuss below, the eight triangles are stars that are classified as BHB by one classification method and not the other but were ultimately classified as BHBs.

Figure 3 shows that of the 44 candidates, 29 are classified BHB by the $D_{0.15}-$*colour* method, and 23 are classified BHB by the *Scale width–Shape* method. There are 21 stars classified BHB by both methods. A total of ten stars are clas-

No.	S/N	$D_{0.15}(\gamma\delta)$	$b(\gamma\delta)$	$c(\gamma\delta)$	A	B	θ	EW(CaIIK)	[Fe/H]	$V_\odot$	$R_\odot$	Class.
	[Å]$^{-1}$	[Å]	[Å]					[Å]		[km s^{-1}]	[kpc]	
(1)	(2)	(3)	(4)	(5)	(6)	(7)	(8)	(9)	(10)	(11)	(12)	(13)
03	39.96	31.90 ± 0.43	9.44	1.00	0.16	0.025	1.526	0.992 ± 0.13	-1.42 ± 0.16	-210.19 ± 09.49	17.16 ± 1.07	BHB
04	34.59	40.47 ± 0.45	10.09	0.76	0.19	0.013	1.529	1.411 ± 0.13	-1.49 ± 0.27	-256.56 ± 08.20	4.42 ± 0.58	A/BS
05	45.28	24.90 ± 0.33	6.18	0.74	0.13	0.015	1.503	2.726 ± 0.12	-0.99 ± 0.29	-41.56 ± 05.17	7.18 ± 0.45	BHB
06	32.42	26.57 ± 0.41	6.36	0.73	0.16	0.016	1.508	4.098 ± 0.13	0.00 ± 0.51	60.82 ± 10.62	5.28 ± 0.33	BHB
12	23.40	30.43 ± 0.74	8.33	0.88	0.28	0.036	1.517	1.343 ± 0.14	-1.09 ± 0.37	-122.20 ± 13.04	16.56 ± 1.04	BHB
13	45.55	37.64 ± 0.40	10.04	0.85	0.16	0.015	1.524	0.959 ± 0.12	-1.89 ± 0.11	94.01 ± 09.00	8.38 ± 1.13	A/BS
14	33.77	38.67 ± 0.47	10.14	0.82	0.19	0.016	1.524	1.385 ± 0.13	... ...	-74.77 ± 06.16	9.09 ± 0.96	A/BS
16	21.95	32.93 ± 0.69	8.94	0.87	0.27	0.031	1.518	1.608 ± 0.15	-1.31 ± 0.28	-85.53 ± 08.73	22.99 ± 1.44	BHB
17	15.22	37.35 ± 1.10	11.23	1.01	0.44	0.053	1.531	1.374 ± 0.17	-1.23 ± 0.31	-46.94 ± 17.74	7.61 ± 0.90	A/BS
18	12.51	25.45 ± 1.28	5.99	0.67	0.47	0.050	1.509	2.668 ± 0.18	-1.13 ± 0.26	-38.52 ± 14.58	55.48 ± 3.47	BHB?
20	25.18	34.61 ± 0.65	8.07	0.70	0.26	0.019	1.522	1.286 ± 0.14	-1.67 ± 0.24	102.15 ± 09.83	6.83 ± 0.93	A/BS
21	28.40	36.53 ± 0.53	8.54	0.72	0.21	0.015	1.525	1.402 ± 0.14	-1.88 ± 0.21	73.66 ± 05.07	4.91 ± 0.77	A/BS
22	15.09	26.39 ± 1.16	6.39	0.72	0.45	0.048	1.509	1.861 ± 0.18	-1.50 ± 0.24	-1.47 ± 12.58	47.12 ± 2.95	BHB
24	70.09	28.30 ± 0.23	8.94	1.16	0.08	0.019	1.529	0.565 ± 0.11	-1.58 ± 0.07	-45.74 ± 09.75	7.80 ± 0.49	BHB?
25	27.50	34.55 ± 0.60	8.37	0.74	0.24	0.019	1.524	1.790 ± 0.14	-1.44 ± 0.25	9.73 ± 06.20	6.91 ± 1.00	A/BS
26	30.97	41.41 ± 0.51	11.19	0.86	0.20	0.017	1.530	2.538 ± 0.13	-0.67 ± 0.35	21.22 ± 07.40	2.32 ± 0.30	A/BS
28	44.21	32.60 ± 0.45	9.79	1.05	0.17	0.029	1.527	1.494 ± 0.12	-1.46 ± 0.13	-150.49 ± 07.19	5.98 ± 0.37	BHB?
29	36.83	31.44 ± 0.47	7.41	0.72	0.18	0.015	1.521	2.019 ± 0.13	-1.60 ± 0.11	34.95 ± 04.89	5.43 ± 0.89	A/BS?
30	50.47	31.73 ± 0.28	9.09	0.96	0.11	0.015	1.515	0.575 ± 0.12	... ...	84.78 ± 08.22	6.99 ± 0.44	BHB
31	24.74	33.37 ± 0.59	9.61	0.97	0.23	0.033	1.516	0.948 ± 0.14	-1.33 ± 0.36	-31.73 ± 07.07	17.57 ± 1.10	BHB
32	36.99	31.38 ± 0.52	9.72	1.12	0.18	0.035	1.533	1.104 ± 0.13	-1.47 ± 0.14	27.57 ± 08.63	8.14 ± 0.51	BHB?
33	17.23	44.10 ± 1.05	11.98	0.88	0.41	0.035	1.533	1.321 ± 0.16	-1.71 ± 0.12	-236.21 ± 12.42	12.51 ± 1.76	A/BS
35	30.54	29.52 ± 0.44	8.53	0.98	0.17	0.027	1.512	0.657 ± 0.13	... ...	-124.38 ± 09.08	9.94 ± 0.62	BHB
36	70.46	29.53 ± 0.21	8.57	0.97	0.08	0.013	1.510	0.407 ± 0.11	... ...	-79.52 ± 10.22	8.08 ± 0.51	BHB
42	34.81	33.70 ± 0.49	7.97	0.72	0.19	0.014	1.522	4.973 ± 0.13	0.00 ± 0.00	18.81 ± 14.56	2.85 ± 0.45	A/BS
43	17.93	31.68 ± 1.08	7.96	0.78	0.44	0.039	1.517	1.028 ± 0.16	-1.77 ± 0.10	160.75 ± 15.77	16.69 ± 1.04	BHB
44	19.96	28.90 ± 0.85	6.88	0.72	0.33	0.030	1.513	1.515 ± 0.15	-1.72 ± 0.11	104.07 ± 10.50	34.63 ± 2.17	BHB
47	39.99	37.10 ± 0.43	8.90	0.73	0.17	0.012	1.525	2.058 ± 0.13	-1.37 ± 0.12	18.68 ± 06.50	5.59 ± 0.84	A/BS
48	32.27	29.68 ± 0.44	8.58	0.98	0.17	0.027	1.509	0.681 ± 0.13	... ...	191.31 ± 09.09	9.62 ± 0.60	BHB
49	71.92	32.40 ± 0.25	9.95	1.09	0.10	0.018	1.530	0.653 ± 0.11	-1.84 ± 0.11	-179.80 ± 15.74	9.44 ± 0.59	BHB?
51	10.34	35.38 ± 1.68	8.46	0.72	0.69	0.050	1.520	1.447 ± 0.20	-1.68 ± 0.23	-9.55 ± 18.51	8.12 ± 1.17	A/BS?
58	16.50	26.50 ± 0.89	6.51	0.71	0.35	0.038	1.504	1.335 ± 0.16	-1.57 ± 0.25	70.13 ± 14.54	37.35 ± 2.34	BHB
63	12.25	37.52 ± 1.42	9.23	0.72	0.55	0.046	1.526	0.506 ± 0.18	-2.93 ± 0.08	-184.24 ± 21.74	12.19 ± 1.99	A/BS?
64	27.34	23.89 ± 0.60	5.22	0.62	0.30	0.049	1.505	2.034 ± 0.14	-1.17 ± 0.43	38.66 ± 12.05	19.34 ± 1.21	BHB?
66	40.67	25.95 ± 0.38	5.81	0.67	0.14	0.013	1.510	1.619 ± 0.12	-1.83 ± 0.20	-16.48 ± 06.52	7.47 ± 0.47	BHB
67	34.66	28.71 ± 0.44	7.22	0.78	0.18	0.018	1.508	1.905 ± 0.13	-1.28 ± 0.13	-214.94 ± 06.28	11.41 ± 0.71	BHB
68	27.66	41.95 ± 0.63	11.21	0.85	0.25	0.021	1.529	1.462 ± 0.14	-1.11 ± 0.17	-218.00 ± 08.86	12.89 ± 1.50	A/BS
70	32.80	30.96 ± 0.43	8.69	0.93	0.17	0.023	1.514	1.486 ± 0.13	-1.12 ± 0.34	-95.59 ± 06.81	18.70 ± 1.17	BHB
72	15.00	25.67 ± 1.09	6.27	0.68	0.45	0.045	1.502	2.263 ± 0.18	-1.31 ± 0.25	49.97 ± 17.98	24.22 ± 1.52	BHB
73	15.53	26.14 ± 0.99	8.14	1.13	0.41	0.089	1.494	0.374 ± 0.19	-1.71 ± 0.44	-10.93 ± 17.91	17.24 ± 1.08	BHB
74	12.07	25.67 ± 1.30	5.53	0.58	0.50	0.036	1.511	2.659 ± 0.18	-1.04 ± 0.28	100.23 ± 15.48	50.10 ± 3.14	BHB?
75	15.93	32.21 ± 0.98	8.83	0.88	0.38	0.044	1.521	1.171 ± 0.17	-2.06 ± 0.15	-11.71 ± 15.06	11.14 ± 0.70	BHB
76	20.07	33.22 ± 0.84	7.79	0.71	0.33	0.024	1.523	2.308 ± 0.15	-1.29 ± 0.12	53.50 ± 07.38	11.27 ± 1.74	A/BS
77	11.21	41.70 ± 1.64	11.80	0.93	0.72	0.066	1.520	1.346 ± 0.19	-1.71 ± 0.23	-1.98 ± 16.19	18.60 ± 2.63	A/BS?
78	54.50	31.09 ± 0.31	8.75	0.93	0.12	0.017	1.519	1.879 ± 0.12	-1.26 ± 0.14	64.57 ± 03.66	10.06 ± 0.63	BHB
79	16.84	35.34 ± 1.10	8.73	0.76	0.46	0.035	1.523	1.387 ± 0.16	-1.82 ± 0.20	-17.16 ± 18.60	5.79 ± 0.87	A/BS
80	13.43	29.85 ± 1.20	6.57	0.61	0.48	0.040	1.516	2.778 ± 0.17	-0.74 ± 0.34	-13.19 ± 20.07	39.86 ± 2.49	BHB?
81	48.89	29.55 ± 0.34	8.59	0.98	0.12	0.021	1.519	1.000 ± 0.12	-1.74 ± 0.11	84.43 ± 07.77	13.26 ± 0.83	BHB
82	22.99	31.67 ± 0.65	8.92	0.92	0.26	0.034	1.516	1.393 ± 0.14	... ...	40.56 ± 08.55	11.75 ± 0.74	BHB
83	26.32	27.84 ± 0.62	7.16	0.79	0.23	0.028	1.513	2.077 ± 0.14	-1.48 ± 0.12	-25.56 ± 05.57	17.97 ± 1.12	BHB
87	12.54	26.92 ± 1.33	5.67	0.61	0.51	0.034	1.515	1.618 ± 0.18	-1.71 ± 0.22	-66.15 ± 17.24	50.53 ± 3.16	BHB?
88	39.76	28.17 ± 0.41	6.29	0.66	0.15	0.012	1.515	1.588 ± 0.13	-1.88 ± 0.10	-114.59 ± 07.40	6.81 ± 1.14	A/BS?
92	95.40	27.89 ± 0.17	8.56	1.09	0.06	0.013	1.516	0.595 ± 0.11	-1.52 ± 0.06	-48.73 ± 10.09	5.27 ± 0.33	BHB?
93	32.73	32.11 ± 0.43	8.80	0.88	0.17	0.020	1.514	1.088 ± 0.13	... ...	-147.60 ± 09.00	9.33 ± 0.58	BHB
94	15.04	29.84 ± 1.22	8.65	0.98	0.44	0.074	1.515	0.403 ± 0.18	... ...	13.16 ± 22.97	19.33 ± 1.21	BHB
96	31.72	30.63 ± 0.56	7.12	0.70	0.22	0.017	1.516	2.394 ± 0.13	-1.34 ± 0.12	-51.85 ± 06.27	6.34 ± 1.02	A/BS
99	36.32	30.68 ± 0.40	8.74	0.95	0.15	0.023	1.513	0.700 ± 0.13	-1.78 ± 0.20	-56.20 ± 06.98	19.24 ± 1.20	BHB
100	94.98	30.73 ± 0.17	9.62	1.13	0.06	0.012	1.526	0.717 ± 0.11	-1.57 ± 0.16	-113.25 ± 08.80	5.68 ± 0.36	BHB
102	50.83	33.12 ± 0.42	9.67	0.99	0.15	0.023	1.528	0.986 ± 0.12	-1.58 ± 0.14	-5.25 ± 08.00	17.35 ± 1.09	BHB

Table 4. Spectroscopic data for the BHB star candidates. The columns (3) to (8) and (11) are the same as in Table 3. In addition, columns (1) and (2) give the number of the star and the spectrum continuum S/N per Å. Column (9) is EW of the CaII K line and column (10) is the measured metallicity for each star with its error. The heliocentric distance is shown in column (12). Finally, the classification of the star is provided in column (13).

sified BHB by one or other of the methods. There is clearly close agreement between the two classification methods. For the ambiguous classifications we combine the information provided by all the parameters. The uncertainties on each parameter define the 2D probability distribution functions for any point. By integrating these functions below the classification boundary we can compute a probability $P(BHB)$ that any star is BHB. Of the nine stars with ambiguous classification eight are classified BHB. We also classify the remaining 15 stars with inadequate spectroscopic S/N, but for these the classifications are given as BHB? or A/BS? to indicate that they are not reliable. We note that the four radial velocity standards (Table 2), previously classified BHB from high–resolution spectroscopy, are all unambiguously classified BHB in both plots.

5 RESULTS

Of the 96 selected candidates only 44 have suitable spectroscopic S/N and Hγ EW for reliable classification. The classification of these 44 candidates results in 29 BHB stars. We have nevertheless followed the classification procedures for the remaining 52 objects, but for clarity have omitted them from Figures 2 and 3. For these objects the final classifications are flagged as questionable. The results of the measurements for all the candidate BHB stars are provided in Table 4.

Table 5 contains a summary of the kinematic properties of the final sample of 29 reliably classified BHB stars. Listed are the identification, RA and Dec., heliocentric velocity and distance, Galactic coordinates l and b and the Galactocentric distance and radial velocity R_{gal} and V_{gal} respectively. To convert the heliocentric quantities to Galactocentric quantities, the heliocentric radial velocities are first corrected for solar motion by assuming a solar peculiar velocity of (U, V, W) = (-9,12,7), where U is directed outward

No.	RA (J2000)	Dec.	$V_\odot$	$R_\odot$	l	b	R_{gal}	V_{gal}
	[°]	[°]	[km s^{-1}]	[kpc]	[°]	[°]	[kpc]	[km s^{-1}]
(1)	(2)	(3)	(4)	(5)	(6)	(7)	(8)	(9)
03	248.9343414	0.1800683	-210.19 ± 09.49	17.16 ± 1.07	16.0580	29.8770	11.39	-143.55
05	229.9829712	0.2714026	-41.56 ± 05.17	7.18 ± 0.45	2.1616	45.3792	5.91	-24.11
06	180.9126129	0.0895671	60.82 ± 10.62	5.28 ± 0.33	277.9714	60.6244	9.28	-45.17
12	239.8858643	-0.1522919	-122.20 ± 13.04	16.56 ± 1.04	9.7586	37.2616	11.42	-79.61
16	229.8426208	-0.3234651	-85.53 ± 08.73	22.99 ± 1.44	1.3890	45.1006	18.25	-70.26
22	229.5568085	0.1586571	-1.47 ± 12.58	47.12 ± 2.95	1.6456	45.6312	41.92	14.49
30	210.7175751	0.3365301	84.78 ± 08.22	6.99 ± 0.44	338.5038	58.1867	7.62	50.33
31	229.4858856	0.4894420	-31.73 ± 07.07	17.57 ± 1.10	1.9410	45.8996	13.31	-14.97
35	210.7082367	0.0929688	-124.38 ± 09.08	9.94 ± 0.62	338.2509	57.9829	9.19	-159.59
36	229.4539948	-0.1177904	-79.52 ± 10.22	8.08 ± 0.51	1.2502	45.5293	6.22	-64.68
43	239.3611908	-0.3381351	160.75 ± 15.77	16.69 ± 1.04	9.1860	37.5826	11.56	201.41
44	248.5698090	-0.1052531	104.07 ± 10.50	34.63 ± 2.17	15.5566	30.0370	28.30	168.95
48	239.3440247	0.3121248	191.31 ± 09.09	9.62 ± 0.60	9.8454	37.9719	6.08	233.88
58	229.0891724	0.1762543	70.13 ± 14.54	37.35 ± 2.34	1.2279	45.9976	32.28	84.87
66	217.5550232	0.1511529	-16.48 ± 06.52	7.47 ± 0.47	348.3371	54.0754	6.07	-33.16
67	239.2290192	-0.4766546	-214.94 ± 06.28	11.41 ± 0.71	8.9468	37.6097	7.16	-175.04
70	229.0451965	-0.1293136	-95.59 ± 06.81	18.70 ± 1.17	0.8546	45.8307	14.33	-81.89
72	210.3879852	0.3614573	49.97 ± 17.98	24.22 ± 1.52	337.9907	58.3777	21.50	14.72
73	217.5059052	0.3670563	-10.93 ± 17.91	17.24 ± 1.08	348.5063	54.2734	12.11	-27.09
75	239.1218567	0.0064421	-11.71 ± 15.06	11.14 ± 0.70	9.3660	37.9773	6.28	29.36
78	248.2692719	-0.3074609	64.57 ± 03.66	10.06 ± 0.63	15.1744	30.1850	5.56	128.09
81	248.2459106	-0.3497654	84.43 ± 07.77	13.26 ± 0.83	15.1186	30.1823	11.66	147.76
82	210.3329315	-0.0795943	40.56 ± 08.55	11.75 ± 0.74	337.4755	58.0257	8.43	3.84
83	229.0241089	-0.1868408	-25.56 ± 05.57	17.97 ± 1.12	0.7725	45.8088	12.12	-12.09
93	210.0473328	0.0858782	-147.60 ± 09.00	9.33 ± 0.58	337.1651	58.3123	6.88	-184.58
94	217.1094971	0.4875866	13.16 ± 22.97	19.33 ± 1.21	348.1101	54.6178	16.20	-3.71
99	229.0039825	-0.2001127	-56.20 ± 06.98	19.24 ± 1.20	0.7391	45.8152	14.82	-42.82
100	248.0934448	-0.2781225	-113.25 ± 08.80	5.68 ± 0.36	15.0951	30.3495	4.53	-50.08
102	248.0232239	-0.1998732	-5.25 ± 08.00	17.35 ± 1.09	15.1287	30.4506	11.58	57.99

Table 5. Summary of positional and kinematic information for the BHB stars. Listed are the: identification, RA and Dec., heliocentric velocity and distance, Galactic coordinates l and b, and the Galactocentric distance and radial velocity R_{gal} and V_{gal} respectively.

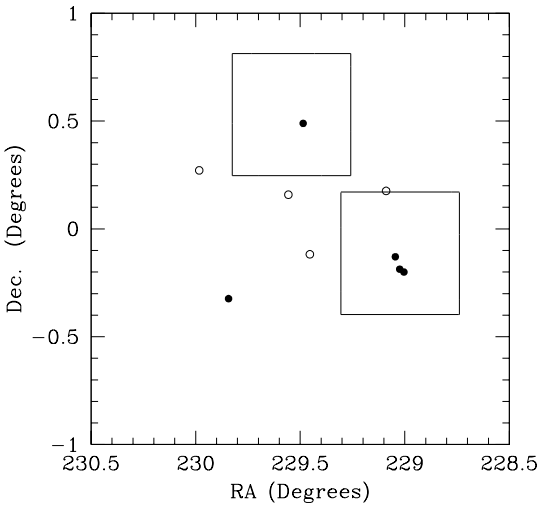

Figure 4. Plot of the BHB stars with similar RA and DEC. as the Pal 5 globular cluster. The two squares are regions of Pal 5 taken from Koch et al. (2004) denoting the centre of Pal 5 (229.0,-0.1) and the trailing stream (229.5,0.5). The filled circles are stars at a similar distance and are therefore most likely to be associated with the globular cluster.

from the Galactic Centre, V is positive in the direction of Galactic rotation at the position of the Sun, and W is positive toward the North Galactic Pole. We have assumed a circular speed of 220 km s^{-1} at the Galactocentric radius of the Sun ($R_{gal} = 8.0$ kpc).

5.1 Comparisons with previous observations of Palomar 5

Our survey passes over the globular cluster Palomar (Pal) 5 (RA= 229.022083°, Dec.=−0.111389° [J2000]). This system has a Heliocentric radial velocity, $V_\odot = -58.7 \pm 0.20$ km s^{-1} (Odenkirchen et al. 2002), a distance $R_\odot$ =23.2 kpc and [Fe/H] = −1.41 (Harris 1996; Clement at al. 2001). Pal 5 is remarkable as observations from the SDSS show a pair of tidal tails, which extend around 4 kpc in opposite directions from the cluster and contain more stars than the cluster itself (Odenkirchen et al. 2003; Koch et al. 2004).

We compare our measurements of BHB stars around Pal 5 to previous work in the literature. There are four stars (numbers 99,83,70,31; shown as filled circles within the boxes in Figure 4) that are plausibly associated with Pal 5, i.e. they are located either within the projected central region of the cluster or in one of the tidal tails. For these four stars we measure a mean heliocentric velocity of −52.3 ± 31.8 and a mean metallicity of −1.43 ± 0.27. These values are entirely consistent, albeit with large errors, with the measures by Harris (1996) and Odenkirchen et al. (2003). However the mean distances (18.4 ± 0.7 kpc) are inconsistent with those reported in Harris (1996). Three of the four stars (numbers 99,83,70) are located in the central position (see Figure 4) at distances 19.2, 18.0, 18.7 respectively (mean = 18.6 ± 0.6). The remaining star that could plausibly be in the stream (number 31) is at 17.57 ± 1.1 kpc. We investigate this apparent distance discrepancy further.

The QUEST survey of RR Lyrae stars (Vivas et al. 2004) found five previously observed RR Lyrae stars in Pal 5 in the V band; the data for these stars are presented in Table 6. The stars in this table are 0.24 magnitudes fainter than our BHB stars, suggesting they are more distant. Assuming an absolute magnitude of the RR Lyraes of $M_V(RR) = 1.112 + 0.214$[Fe/H] (as we discuss in §4.1), and an [Fe/H] = −1.4, then the mean distance of this sample is 21.2 ± 0.93 kpc.

Two further Pal 5 HB stars are available online via the

ID	R.A. (J2000)	Dec.	V	$B-V$	$R_\odot$	Refs.
399	15 15 57.25	-00 06 52.8	17.44	0.03	21.16	(1), (2)
400	15 15 57.97	-00 11 23.1	17.33	0.01	20.11	(1)
401	15 15 58.31	-00 05 47.3	17.58	0.03	22.57	(1)
402	15 16 05.79	-00 11 12.3	17.46	0.04	21.36	(1)
404	15 16 12.79	-00 10 02.7	17.38	0.03	20.58	(1)

Table 6. Summary of position, colour, magnitude and distance of RR Lyrae stars observed in the QUEST survey (Vivas et al. 2004). References: (1) Kinman & Rosino (1962); (2) Clement et al. (2001); (2) Wu et al. (2005)

ID	V	$B-V$	$R_\odot$
31	17.185 ± 0.014	0.043 ± 0.0166	17.57
70	17.238 ± 0.016	0.083 ± 0.0174	18.70
83	17.036 ± 0.016	0.196 ± 0.0147	17.97
99	17.329 ± 0.016	0.067 ± 0.0178	19.24
S41	17.453 ± 0.003	0.103 ± 0.0031	20.02
S40	17.519 ± 0.002	0.087 ± 0.0023	20.33

Table 7. Summary of the magnitude, colours and distances for our stars in the direction of Pal 5. The two stars at the bottom of the table are HB stars in the core of Pal 5.

Canadian Astronomy Data Centre(CADC)[1] which are also observed in the SDSS. Like the QUEST RR Lyrae stars these stars are more than 0.2 magnitudes fainter than the those observed in this paper. Table 7 summarises the colours, and V magnitude of these two stars along with the four stars in our study. If we again assume a metallicity of -1.4 then the stars s41 and s40 are at 20.0 and 20.3 kpc respectively. We note for completeness that if the distances are derived using the SDSS colours and magnitudes as in §4.1 then we find the stars s41 and s40 are 20.9 and 21.9 kpc respectively.

Therefore, it seems unlikely that our BHB stars in the direction of Pal 5 are part of the core of this cluster. However, the stars 70, 83 and 99 occupy a volume of space of 0.0004 cubic kpc, which is a space density of around 8000 per cubic kpc. Kinman et al. (1994; equation 12) find a mean density of BHB stars at $R_{gal} = 14$ kpc to be approximately 0.9 per cubic kpc. The three stars therefore appear to be in an overdensity perhaps indicating that Pal 5 is extensive not only in the plane of the sky but also in depth. Clearly more observations are required to fully understand this structure and its possible relation to Pal 5 and/or the Sgr stream.

6 DISCUSSION

Table 5 summarises the main observational results of the paper; a sample of BHB stars with measured radial velocities in the vicinity of the Sgr stream. We now investigate whether there is evidence that these stars actually reside in this stream.

In Figure 5 we plot Heliocentric radial velocity and distance versus RA for the 29 BHB stars. In Figure 5(upper) we split the sample into three groups of $R_\odot$: stars at $5 < R_\odot < 14$ kpc (open circles); (ii) stars at $14 < R_\odot < 25$ kpc (filled circles); and stars at $R_\odot > 25$ (open triangles). We overplot on this figure simulations of the tidal stream of Sgr for various halo flatness taken from Martínez-Delgado et al. (2004). The curves on this plot are for values of the axis ratio of the density distribution, q_d, which range from 0.1 to 1.0 (upper to lower curves). However, the axis ratio of the potential, q_p, is the quantity that determines the satellite orbit and hence the shape of the potential. This parameter is a function of q_d and Galactocentric distance (see Fig. 11 in Martínez-Delgado et al. 2004) and ranges from 0.5 (oblate potentials) to 1.0 (spherical potentials).

In Figure 5(lower) we plot $V_\odot$ versus RA for the same three groups of BHB stars. The plot reveals a possible correlation between $V_\odot$ and RA which suggests that 10 of the 12 stars in the region $14 < R_\odot < 25$ kpc could be associated with a stream. It is clear, however, that the velocity distribution of the stars is systematically lower than any of the Martínez-Delgado et al. (2004) models presented here. There could be many reasons for this. One plausible reason is that the Martínez-Delgado model considers only the last (~ 5 Gyr) orbit. As BHB stars are old, any putative stream might feasibly belong to a later orbit that is not considered in this model. In the next section we investigate the evidence that this putative stream is plausibly associated with the Sgr tidal debris.

6.1 Comparisons with previous work

As we briefly discuss in §1 there have been numerous detections of the Sgr tidal tail around the sky using tracers that map different epochs, i.e orbits in which the debris was stripped from the satellite. For example, Majewski et al. (2003, 2004) isolated M giants in the Two Micron All-Sky Survey (2MASS) in order to map the position and velocity distribution of tidal debris from Sgr around the entire Galaxy. In Law, Johnston & Majewski (2005; hereafter LJM05) these stars are compared with numerous simulations of the tidal debris of the Sgr satellite in differing Galactic potentials. We refer the reader to this paper for details of the parameters used in this model. The simulations are created using the relatively young M giants as the principal observable. We note that BHB stars and carbon stars are expected to trace older debris than M giants. We compare these models with our BHB stars and other stellar types that are available.

Before we are able to compare our data with such models we need to convert our coordinates to the system defined in Majewski et al. (2003). In this coordinate system the zero plane of the latitude coordinate $B_\odot$ coincides with

[1] The data is available at: http://cadcwww.dao.nrc.ca/astrocat/ in the Stetson Standard Fields

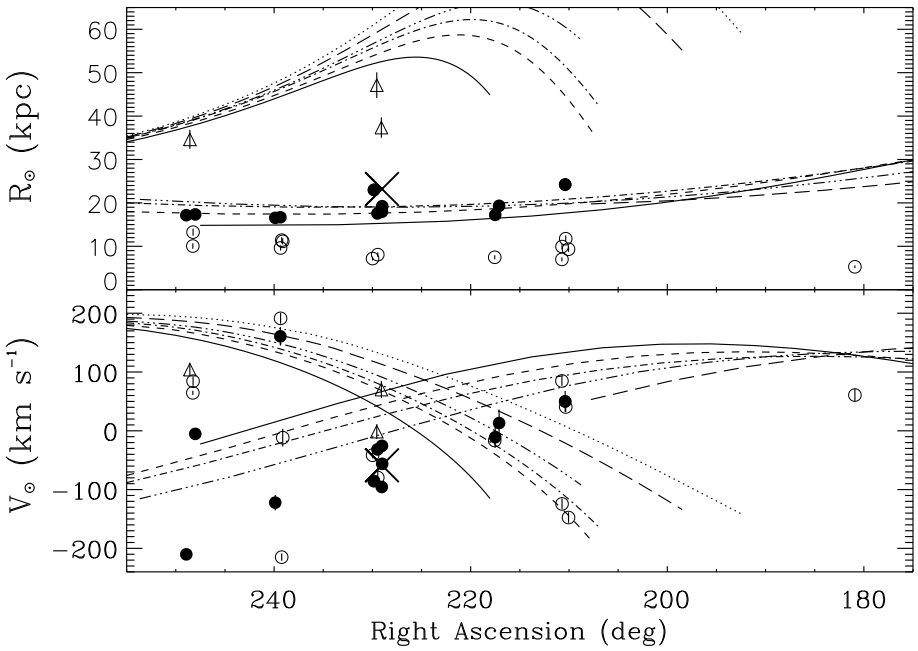

Figure 5. *Upper:* Plot of $R_\odot$ versus RA for the BHB stars. The BHB stars are separated in distance so that stars are at: (i) $5 < R_\odot < 14$ kpc (open circles); (ii) $14 < R_\odot < 25$ kpc (filled circles); and $R_\odot > 25$ (open triangles). The curves are taken from Martínez-Delgado et al. (2004) and describe the axis ratio of the density distribution, q_d. The values of q_d range from 1.0 (dotted line) to 0.1 (solid line) respectively. *Lower:* A plot of $V_\odot$ versus RA for the three groups. The symbols and curves are the same as those on the upper plot.

the best-fit great circle defined by the Sgr debris, as seen from the Sun; the longitudinal coordinate $\Lambda_\odot$ is zero in the direction of the Sgr core and increases along the Sgr trailing stream. Our sample resides in the region $260^\circ < \Lambda_\odot < 320^\circ$ and $-17^\circ < B_\odot < 16^\circ$. This corresponds to a section of the leading portion of the orbit which is particularly sensitive to the halo shape. Indeed, M stars appear to strongly favour models with prolate rather than oblate halos (Helmi 2004). In contrast, by fitting planes to the leading and trailing debris and measuring the orbital precession of the Sgr debris Johnston, Law & Majewski (2005) find oblate halos are favoured.

In Figure 6 we compare our BHB data with the best-fit numerical simulations. Overplotted are various other tracers which we discuss below. The M giants are represented by open stars. Figure 6 illustrates the differences for the halo potential models. We plot distances and radial velocities of the best-fit simulations of the Galactic halo potential, which was created by LJM05 for oblate (q=0.9, upper plots), spherical (q=1.0, middle plots) and prolate (q=1.25, lower plots) potentials. The bold points (green) are old debris stripped four orbits ago whilst faint points (red) are from earlier orbits.

The BHB stars are shown as filled circles, open circles and filled triangles as in Figure 5. The filled circles represent our putative stream. The BHB stars that are shown as open circles do not appear to be associated with the models in either velocity or distance. However, the 10 of 12 filled circles are plausibly associated with the older debris both in velocity and distance in the LJM05 model. More data is required to confirm whether the three distant BHB stars (shown as triangles) are also associated with a more distant younger part of the Sagittarius stream. They do not show a remarkable metallicity which might suggest they are in an earlier orbit of Sgr.

Carbon stars (filled squares) are from the catalogue provided by Totten & Irwin (1998), confining ourselves to the same $\Lambda_\odot$ ranges as the BHB data and to similar distances (improved distance estimates are added from Totten, Irwin & Whitelock 2000). Some of the carbon stars (blue squares) do appear to follow the M stars in velocity, however their distances do not appear to be associated at all. This discrepancy might be due to the uncertainty in distance measurements for individual carbon stars. It is also plausible that the carbon stars trace older debris than the M giants as they can have larger ages. This sample however does not show any correlation with the BHB stars.

The crosses in Figure 6 are eight metal poor K-giants discovered by Kundu et al. (2002) to have coherent, smoothly varying distances and radial velocities. The Kundu et al. (2002) K-giant stars represent relatively old debris stripped from Sgr three pericentric passages ago. The velocities of this sample fit the models reasonably well particularly for the prolate potential shown in Figure 6(lower). However, the distances remain uncertain in all three models.

In summary, the M stars and carbon stars predominantly map out the earlier tidal debris. The velocity data for both tracers appears to qualitatively fit the prolate models rather well (Figure 6, lower). However the distance information is less clear, particularly for the carbon stars. The

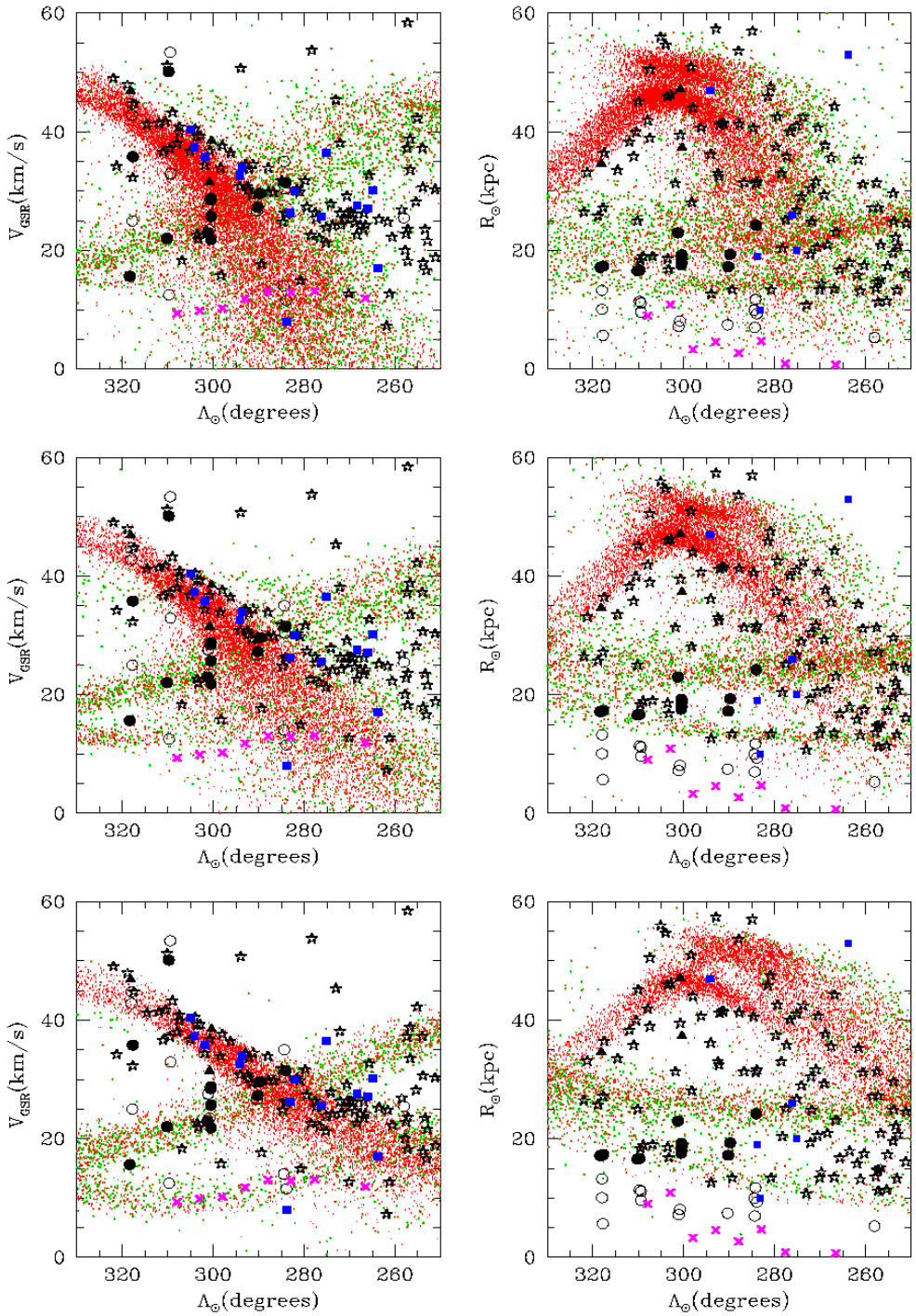

Figure 6. Distances and radial velocities of the best-fit simulations of the Galactic halo potential created by Law, Johnston & Majewski (2005) for oblate potentials (top plots), spherical potentials (middle plots) and prolate potentials (bottom plots). The bold dots (green) are old debris stripped four orbits ago whilst faint dots (red) are from earlier orbits. Overplotted are: BHB observations (as in Fig. 5, i.e. filled and open circles and filled triangles); filled squares are carbon stars selected from Totten & Irwin (1998); open stars are M giants from Majewski et al. (2004) and crosses (magenta) are K-giants from Kundu et al. (2002).

velocity information of the metal poor K-giants again appears to fit the prolate models well but again the distance information does not support this case. The BHB data are too scarce in this study to distinguish competing models of halo flatness despite being comparitively accurate standard candles. We emphasise that these observations are over a section of the leading part of the stream. Conclusive evidence for halo flatness will probably require multi-epoch observational data from leading and trailing debris.

7 SUMMARY

We close with a summary of the main points in this paper. We have presented the first results of a pilot study to trace out the Sgr stream using BHB stars. Spectroscopy of the A-type stars, obtained with the 2dF, produced a sample of 44 stars with data of suitable quality for classification into the classes BHB and A/BS. The final sample (Table 4) comprises 29 stars classified as BHB. The heliocentric distances range from 5 to 47 kpc, with heliocentric radial velocities accurate to 10 km s^{-1}, on average, and distance errors $< 10\%$.

We find 10 of 12 BHB stars at $14-25$ kpc are plausibly tracing a stream. By comparing this data with models from LJM05, we find that these stars may be associated with the older debris of Sgr both in velocity and distance. Further observations along the entire Sgr orbit both along the trailing and leading stream and at greater distances are clearly required to trace the full extent of this structure on the sky. A BHB analogue of the 2MASS survey would complement such surveys by probing the older tidal debris, which may be crucial in constraining the shape of the Galaxy halo (e.g. Helmi 2004). For the BHB stars which reside in the putative stream, we find three of our BHB stars in the direction of the globular cluster Palomar (Pal) 5 appear to be in a foreground overdensity. More observations around these stars are required to establish any link to Pal 5 and/or the Sgr stream itself. Despite these controversies BHB stars have the distinct advantage of being more reliable standard candles than M stars and carbon stars and so the distance estimates are more precise. We emphasise observations of BHB stars have unlimited potential at providing accurate velocity and distance information on distant halo streams. The next generation multi-object spectrographs provide an excellent opportunity to accurately trace the full extent of such structures.

ACKNOWLEDGEMENTS

We would like to thank the referee for a number of helpful comments. We thank David Law and David Martínez-Delgado for providing us with their models. The Sgr coordinate system conversions made use of code at: http://www.astro.virginia.edu/~srm4n/Sgr/code.html. We thank Caroline Van Breukelen for useful comments. The authors acknowledge PPARC for financial support. This paper uses observations made on the Anglo Australian Telescope at Siding Springs using the 2dF instrument. We made use of the SDSS online database. Funding for the creation and distribution of the SDSS Archive has been provided by the Alfred P. Sloan Foundation, the Participating Institutions, the National Aeronautics and Space Administration, the National Science Foundation, the U.S. Department of Energy, the Japanese Monbukagakusho, and the Max Planck Society.

REFERENCES

Alves D. R., 2004, NewA Rev., 48, 659
Arp H. C., 1955, AJ, 60, 317
Arp H. C., 1962, AJ, 135, 311
Bailey J. et al. 2003, http://www.aao.gov.au/2df/manual.html
Beers T. C., Preston G.W, Shectman S.A., Doinidis S.P., Griffin K.E., 1992, AJ, 103, 267
Bellazzini M., Correnti M., Ferraro F.R., Monaco L., Montegriffo P., astro-ph/0512109
Brown W. R., Geller M. J., Kenyon S. J.,Beers T. C., Kurtz M. J., Roll J. B., 2004, AJ, 127, 1555
Brown W. R., Geller M. J., Kenyon S. J., Kurtz M. J., Allende P. C., Beers T. C., Wilhelm R., 2005, AJ, 130, 1097
Cacciari C., Clementini G., LNP, 635, 105
lement C.M., 2001, AJ, 122, 2587
Clementini G., Gratton R., Bragaglia A., Carretta E., Di Fabrizio L., Maio M., 2003, ApJ, 125, 1309
Clewley L., Warren S.J., Hewett P.C., Norris J.E., Peterson R.C., Evans N.W., 2002, MNRAS, 337, 87
Clewley L., Warren S.J., Hewett P.C., Norris J.E., Evans N.W., 2004, MNRAS, 352, 285
Clewley L., Warren S.J., Hewett P.C., Norris J.E., Evans N.W., 2005, MNRAS, 362, 349
Cudworth K.M., 1979, AJ, 84, 1866
Dohm-Palmer R. C. et al. 2001, ApJ, 555, L37
Fukugita M. et al., 1996, AJ, 111, 1748
Gould A., Popowski P., 1998, ApJ, 508, 844
Harris W.E. 1996, AJ, 112, 1487
Helmi A., 2004, ApJ, 610, 97
Ibata R. A., Gilmore G. and Irwin M. J., 1994, Nature, 370, 6486, 194
Ibata R., Chapman S., Ferguson A.M.N., Irwin M., Lewis G., McConnachie A., 2004, MNRAS, 351, 117
Irwin M., Hatzidimitriou D., 1995, MNRAS, 277, 1354
Ivezić, Ž et al., 2000, AJ, 120, 963
Johnston K.V., Law D.R., Majewski S.R., 2005, ApJ, 619, 800
Johnston K.V., Zhao H., Spergel D.N., Hernquist L., 1999, ApJ, 512, L109
Kinman T.D., Rosino L., 1962, PASP, 74, 499
Kinman T.D., Suntzeff N.B., Kraft R.P., 1994, AJ, 108, 1722
Koch A. et al., 2004, AJ, 128, 2274
Kundu A. et al., 2002, ApJ, 576, L125
Law D.R., Johnston K.V., Majewski S.R., 2005, ApJ, 619, 807
Lewis I. J., Cannon R. D., Taylor K. et al., 2002, MNRAS, 333, 279
Majewski S.R. et al., 2003, ApJ, 599, 1082
Majewski S.R. et al., 2004, AJ, 128, 245
Martínez-Delgado D. and Gómez-Flechoso M. Á., Aparicio A., Carrera R, 2004,ApJ, 601, 242

Monaco L., Bellazzini M., Ferraro F. R., Pancino E., 2003, ApJ, 597, 25
Newberg, H. J., et al. 2002, ApJ, 569, 245
Odenkirchen M., Grebel E. K., Dehnen W., Rix H.W., Cudworth K. M.,2002, AJ, 124, 1497
Odenkirchen M. et al., 2003, AJ, 126, 2385
Peterson R.C, 1983, ApJ, 275, 737
Pier J.R, 1983, ApJS, 53, 791
Preston G.W., Shectman S.A., Beers T.C., 1991, ApJ, 375, 121
Schlegel D.J., Finkbeiner, D.P., Davis, M., 1998, ApJ, 500, 525
Sirko E., Goodman J., Knapp G.R., Brinkmann J., Ivezić, Ž., Knerr E.J., Schlegel D., Schneider D.P., York D.G., 2004, AJ, 127, 899
Smith, J. A. et al. 2002, AJ, 123, 2121
Totten, E.J., Irwin, M.J., 1998, MNRAS, 294, 1
Totten, E.J., Irwin, M.J., Whitelock, P.A., 2000, MNRAS, 314, 630
Vivas A.K. et al., 2001, ApJ, 554, L33
Vivas A.K. et al., 2004, AJ, 127, 1158
Vivas A.K., Zinn R., Gallart C., 2005, AJ, 129, 189
Wu C., Qiu Y. L., Deng J. S., Hu J. Y., Zhao Y. H., 2005, AJ, 130, 1640
Yanny B. et al., 2000, AJ, 540, 825